

Correlation between luminescence and structural evolution of colloidal silicon nanocrystals synthesized under different laser fluences

W S Wu¹, H L Hao^{1,3} , Y X Zhang¹, J Li¹, J J Wang¹ and W Z Shen^{2,3}

¹ College of Material Engineering, Shanghai University of Engineering Science, 333 Long Teng Road, Shanghai 201620, People's Republic of China

² Institute of Solar Energy, and Key Laboratory of Artificial Structures and Quantum Control (Ministry of Education), Department of Physics and Astronomy, Shanghai Jiao Tong University, 800 Dong Chuan Road, Shanghai 200240, People's Republic of China

E-mail: sulee8866@126.com and wzshen@sjtu.edu.cn

Received 5 September 2017, revised 20 October 2017

Accepted for publication 24 October 2017

Published 11 December 2017



CrossMark

Abstract

We present a detailed investigation of the structural evolution and photoluminescence (PL) properties of colloidal silicon (Si) nanocrystals (NCs) synthesized through femtosecond laser ablation at different laser fluences. It is shown that the mean size of colloidal Si NCs increases from ~ 0.97 – 2.37 nm when increasing laser fluence from 1.0 – 2.5 mJ cm^{-2} . On the basis of structural characterization, temperature-dependent PL, time-resolved PL, and PL excitation spectra, we identify that the size-dependent spectral shift of violet emission is attributed to the quantum confinement effect. The localized excitons' radiative recombination via the oxygen-related surface states on the surface of the colloidal Si NCs is employed to explain the origin of the blue emission.

Keywords: colloidal silicon nanocrystals, femtosecond laser ablation, laser fluence, surface engineering, photoluminescence

(Some figures may appear in colour only in the online journal)

In recent years, colloidal silicon (Si) nanocrystals (NCs) have attracted tremendous research interests due to their intriguing optical and electronic properties and promising applications in optoelectronic devices [1–4], solar cells [5–8], as well as fluorescent biomarkers [9–11]. The fascinating applications of colloidal Si NCs in these aspects are mainly because of their non-toxicity, abundance, continuous tunability of photoluminescence (PL) over a broad spectral range from UV to near-IR, and high compatibility with microelectronics [12]. Compared with traditional chemical and physical synthesis procedures for colloidal Si NCs, pulsed laser ablation (PLA) in liquid has been proven to be a green and convenient method without any un-necessary by-products [13, 14].

Under laser ablation, the plasma plume formed and confined within the liquid media is an ideal environment to promote non-equilibrium processes, which is beneficial to the formation of colloidal Si NCs. The versatile one-pot synthesis of organic-capped colloidal NCs (e.g., Si, germanium, gold, copper) through PLA can be formed by the automatic reaction between the reactive nanocrystalline surface with surface radicals and the reactive unsaturated organic molecules [15–19].

As we know, various laser parameters, such as liquid media, laser wavelength, pulse duration, and pulse energy, should be taken into account to control the structure and surface chemistry of Si NCs, which can further determine the nature of luminescence [20–25]. Moreover, it has been both experimentally and theoretically shown that the surface

³ Authors to whom any correspondence should be addressed.

chemistry indeed affect the color of the light emission from Si NCs [26, 27]. Among these parameters, laser fluence is a very important parameter to modify directly the Si NCs size, chemical configurations and growth mechanism [24]. Yang *et al* [20] and Chewchinda *et al* [25] have reported that the mean size of colloidal Si NCs produced by nanosecond pulsed laser decreases with the increase of laser energy, resulting in the blueshift of luminescence. Nevertheless, Intartaglia *et al* [23] and Hamad *et al* [24] have drawn the contrary conclusions, the mean size of Si NCs synthesized using femtosecond pulsed laser increases with increasing laser energy. The above different data trend from Si NCs fabricated by nanosecond and femtosecond laser ablation can be explained as the following: (i) On a time scale, nanosecond laser pulses usually release energy slowly compared with the thermal relaxation processes of the target, while femtosecond laser pulses release energy to electrons in the target much faster than electron–phonon thermalization processes, which can reduce local heating on the target [23]. Moreover, the temporal overlap between laser pulse duration and material evaporation time induces thermodynamic instability of the plasma plume [28]. As a consequence, there are some differences in the generated nanoparticles produced by means of nanosecond and femtosecond laser pulse duration.

(ii) For nanosecond laser pulses, the production of silicon atoms filled in the plasma plume is less at low laser fluence, the pressure and temperature of plasma plume is low at this stage. Therefore, the nucleation is relatively difficult. The small number of nuclei formed consumes the surrounding silicon clusters, resulting in the formation of large size silicon particles [20]. Under high laser fluence, the pressure and temperature of the formed plasma plume is relatively high, which is favorable to the formation of silicon nuclei in all the plume region. The incrementally supplied silicon atoms are shared by more nuclei, leading to the small sized silicon nanoparticles.

In the case of femtosecond laser pulses, low laser fluence can generate a sustainable cavitation bubble, which subsequently develops higher pressure favorable to the formation of smaller sized Si nanoparticles. Nevertheless, the cavitation bubble cannot sustain for a long time for the high laser fluence case, the pressure across the bubble is lower due to its collapse, resulting in the aggregation for the produced Si NCs [24, 29]. Therefore, it is essential to have a deep insight into the effect of laser fluence on the structure and optical properties of colloidal Si NCs.

Up to date, most of the reported light emission resulting from colloidal Si NCs fabricated by PLA is limited in the blue range. It has been usually assigned to quantum confinement effect (QCE) [30], direct-transition-like recombination of quantum-confined electron–hole pairs [31], and oxide-related radiative recombination of electron–hole pairs via surfaces of colloidal Si NCs [32]. In our previous work, we have proposed that the surface chemistry of the Si NCs in terms of introducing localized states is also an important factor affecting the light emission [33]. The present work aims to clarify the luminescence mechanism of violet and blue emission resulting from colloidal Si NCs with controllable

sizes and surface passivation. The radiative recombination of electron–holes pairs from colloidal Si NCs is expected to exhibit different characteristics within the different wavelength ranges, which not only provides ways to identify the luminescence mechanism of the Si NCs, but also realizes the possibility to control the visible light in desired wavelength range for Si-based optoelectronics devices.

During preparing colloidal Si NCs, the mixture of porous silicon powder (25 mg) with a mean diameter of 100–120 nm (Aladdin) and 1-octadecene (5 ml, >99%, Aladdin) was ultrasonically for 1 h. The irradiation was performed by a femtosecond (fs) pulsed Ti/sapphire laser operated at 800 nm with pulse duration of 100 fs and frequency of 80 MHz. The laser beam was focused on the above mixture with a spot size around 2 mm in diameter using a lens with a focal length of 10 cm. The irradiation time was maintained at 1 h and the solution was continuously stirred by a magnetic stirrer during laser irradiation. After irradiation for 1 h, the supernatant liquid was filtered by centrifugation at 12 000 rpm with a membrane filter that had a pore size 200 nm for 30 min and the colloidal Si NCs were prepared. The studied samples were named by S_x ($x = 1, 2, 3, 4$) for laser fluence at 1.0, 1.5, 2.0 and 2.5 mJ cm^{-2} , respectively.

The formation and morphology of the samples were examined by x-ray diffraction (XRD, Philips X'pert) using Cu K α line (0.154 19 nm) and high resolution transmission electron microscopy (HRTEM, JEOL JEM-2100F). Raman scattering spectra were performed on a Jobin Yvon LabRAM HR 800 UV micro-Raman spectrometer using 514.5 nm line of Ar ion laser. Fourier transform infrared (FTIR) spectra were measured at Nicolet Nexus 870 FTIR spectrometer within 400–4000 cm^{-1} range. The bonding configurations were analyzed by x-ray photoelectron spectroscopy (XPS) spectra with a Shimadzu Kratos Axis Ultra DLD spectrometer using a monochromatic Al K α x-ray source (1486.6 eV), and UV–visible (UV–vis) absorption spectra were measured by a Perkin-Elmer Lambda 20 spectrometer. Steady-state PL and PL excitation (PLE) spectra were recorded by Edinburgh Instruments FLS920 through normalizing the variation in Xe lamp output over the spectral range of interest. Time-resolved PL was measured by using a 405.0 nm diode laser with a pulse width of 60.0 ps as the excitation source.

Figure 1(a) displays XRD patterns of all the samples produced in 1-octadecene at different laser fluences. The broad diffraction peaks at around 28.5°, 47.6°, 56.5°, 76.4° and 89.2° are indexed to silicon phase with diamond structure (JCPDF-27-1402), corresponding to Si (111), Si (220), Si (311), Si (331) and Si (422) planes, respectively. The appearance of broad diffraction peaks is indicative of the formation of Si NCs [34]. In addition, the broad diffraction peak at approximately 20° is from the surface alkyl molecules [35]. With the increase of laser fluence, the intensity of diffraction peaks increases and the full widths at half maximum (FWHM) of those decreases from S1 to S4, indicating that the mean diameter and crystalline degree of Si NCs increase. The average size of Si NCs can be calculated by employing Scherrer equation [35]: $D = K\lambda/\beta \cos \theta$, D is the mean diameter of Si NCs, K is a constant 0.89 for spherical

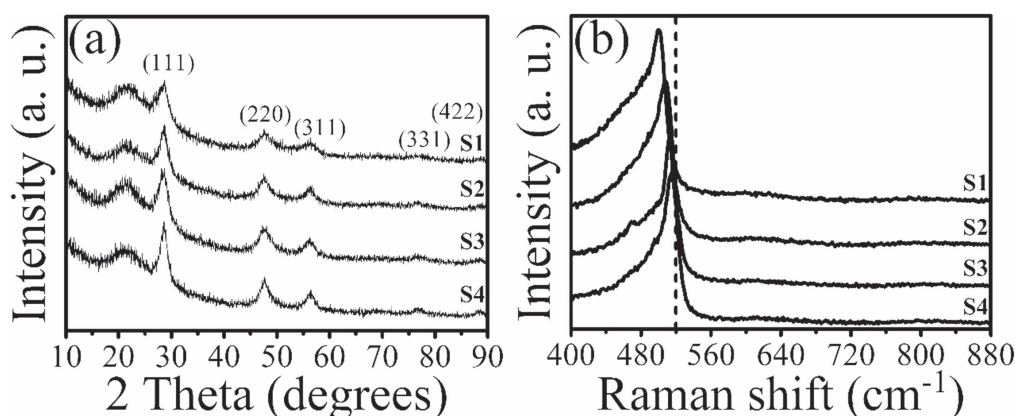


Figure 1. (a) XRD patterns of alkene-passivated Si NCs that were synthesized in 1-octadecene at different laser fluences: 1.0 (S1), 1.5 (S2), 2.0 (S3) and 2.5 mJ cm^{-2} (S4), and (b) Raman spectra of colloidal Si NCs samples as in figure 1(a).

particles, λ is x-ray wavelength of 0.15148 nm, θ is Bragg diffraction angle of the peak, and β is FWHM of the diffraction peak in radians. The determined mean diameters of Si NCs from the corresponding Si (111) diffraction peak are 0.97, 1.43, 1.91, and 2.34 nm for S1–S4, respectively.

Figure 1(b) presents Raman spectra of the Si NCs as in figure 1(a). It is seen that the Raman peak lies at 499, 508, 513 and 515 cm^{-1} for S1–S4, respectively. Due to its zero momentum, the optical phonon of bulk crystalline Si is a Raman active mode and occurs at the center of Brillouin zone to form a sharp peak at 520 cm^{-1} . It can be found that more phonons appear in small Si NCs, rather than at the center of Brillouin zone. This is contributed to the phonon density of states, which leads to the redshift of Raman peak position and Raman spectral broadening of the transverse phonon line compared with bulk crystalline Si [36–38]. The relationship between the redshift of Raman peak position of Si NCs and the mean diameter of Si NCs can be described through the phenomenological law [39, 40]: $\Delta\omega = -19.856/d^{1.586}$, where $\Delta\omega$ represents the redshift of Raman peak position of Si NCs compared with that of bulk Si, and d is the mean diameter of Si NCs. The calculated mean diameters for S1–S4 are 0.96, 1.37, 1.93, and 2.35 nm, respectively, in good agreement with the results from XRD data in figure 1(a).

The detailed information about the morphology, size, and size distribution of Si NCs can be directly characterized by TEM analyses. Due to small atomic number difference between Si and carbon (C) support layer, it is difficult to obtain clear TEM images. Hence, graphene was used to be as a support layer to provide the clear Si NCs TEM images. Before measurements, all the samples were purified rigorously with the mixture of solvent/antisolvent pairs of toluene/acetone for ultrasound 30 min to remove the excess 1-octadecene. The washing procedure was repeated at least five times and then Si NCs were dried in drying oven under vacuum for 24 h at 150 °C. The resulting clean Si NCs were dispersed in ethanol with high volatility for HRTEM measurements.

Figures 2(a)–(d) and (a1)–(d1) show TEM images and the corresponding size distributions of colloidal Si NCs synthesized in 1-octadecene, respectively. It can be observed

that Si NCs are spherical and homogeneously dispersed in 1-octadecene, and the mean size of Si NCs is \sim 0.95, 1.41, 1.92, and 2.37 nm for S1–S4, respectively. The inset in figure 2(a) is a typical HRTEM image of a Si NC of S1 with lattice spacing \sim 0.3 nm, corresponding to (111) plane of cubic Si [23, 41].

The dependence of colloidal Si NCs size on the laser fluence is confirmed to be a size increment when the laser fluence increases. And the similar dependence of Si NCs size on the laser energy has been reported in Si NCs [23, 24]. The variation of Si NCs size with laser energy mainly depends on the cavitation bubble dynamics arising from the target surface. Low laser energy can generate a sustainable cavitation bubble, which develops higher pressure favorable to the formation of smaller sized Si nanoparticles. Whereas, the cavitation bubble cannot sustain for a long time for high laser energy case, the pressure across the bubble is lower due to its collapse under high laser energy, which results in the aggregation for the produced Si NCs [24, 29].

Figure 3(a) presents the FTIR spectra of all samples to directly reveal the chemical bonds inside Si NCs. The absorption bands at 808, 1376, 1465, 1639, 2854, 2923, and 2954 cm^{-1} can be assigned to the Si–O bending, CH_3 bending, Si–C scissoring, Si–O–H, symmetric CH_2 stretching, antisymmetric CH_2 stretching, and asymmetric CH_3 stretching modes, respectively [32, 42, 43]. There are two possible origins for the absorption peak at 680 cm^{-1} , one is Si–H vibration mode and the other is Si–C asymmetric vibration mode [44, 45]. In this work, no absorption peak falling in 2000–2200 cm^{-1} can be observed, suggesting that there are no Si–H bonds on the surface of Si NCs. The absorption peak at 680 cm^{-1} can be assigned to Si–C asymmetric vibration mode on the surface of Si NCs. The appearance of Si–C bonds on the surface of Si NCs indicates that the Si NCs surface has been successfully passivated by organic molecules [46]. The C passivation of Si NCs surface can be explained by cycloaddition chemistry [32]. During laser ablation, the Si NCs will have very high free energy, and some Si atoms on the surface are unsaturated and active under extreme conditions, which can react with surrounding liquid and thus a cyclic compound will be formed. This can be well

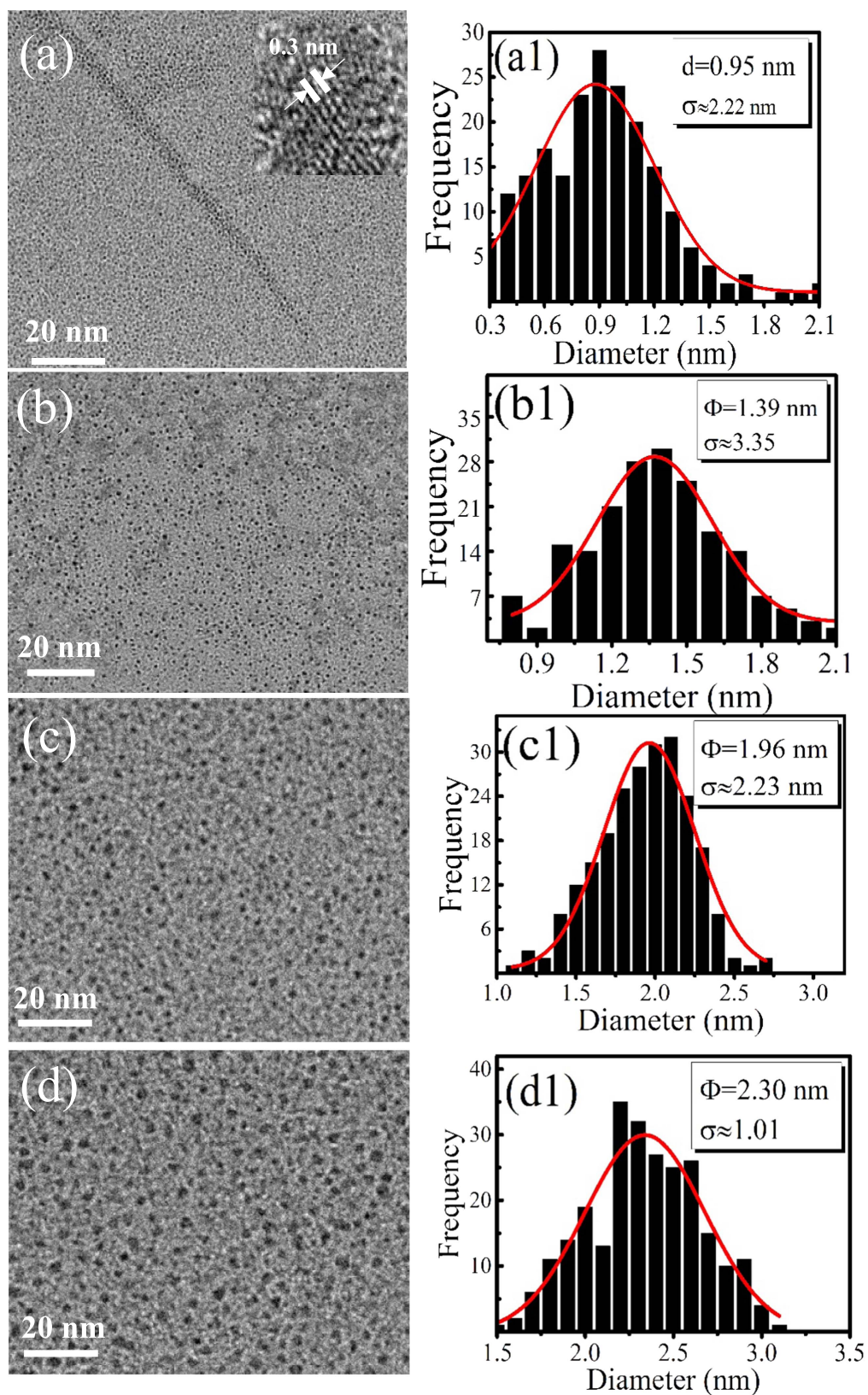


Figure 2. (a)–(d) and (a1)–(d1) TEM images and the corresponding size distribution of colloidal Si NCs as in figure 1(a). Inset: a typical HRTEM image of a Si NC. Φ , mean size; σ , standard deviation.

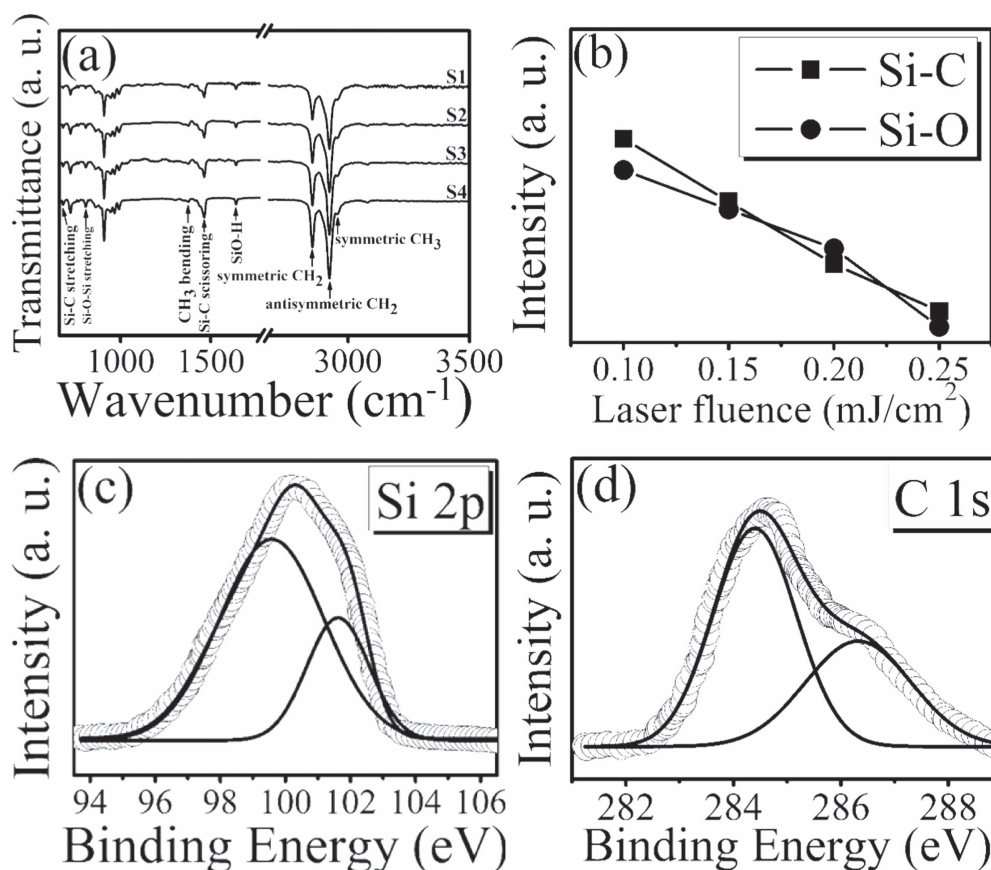


Figure 3. (a) Infrared absorption spectra for colloidal Si NCs samples, (b) the densities of Si–C and Si–O bonds as a function of laser fluence, and the experimental (open circles) and calculated (solid curves) XPS spectra for S4: (c) Si 2p and (d) C 1s.

expressed by the following schematic illustration of chemical reaction in ablation process [32]:

Here, R represents $(\text{CH}_2)_{14}\text{CH}_3$. Therefore, the Si–C and Si–O bonds are expected to be formed at the surfaces of Si NCs. By integrating the infrared absorption bands in figure 3(a), we can observe that the intensities of Si–C and Si–O bonds decrease with laser fluence, as illustrated in figure 3(b). Some Si–C and Si–O bonds would be broken on the surface of Si NCs under the extreme equilibrium conditions at high laser energy.

XPS measurements were performed to determine precisely the chemical configurations of Si NCs and the cover degree of Si–C bonds on the surface of Si NCs. Figures 3(c)–(d) display the representative experimental (open circles) and well Gaussian fitted (solid curves) Si 2p and C 1s core-level binding energy spectra of S4, respectively. It can be observed that Si 2p spectrum can be well fitted by two Gaussian peaks at ~ 99.5 and 102.1 eV. The peak at 99.5 eV is characteristic of pure Si and the peak of 102.1 eV can be attributed to the combination of Si–C and Si–O bonding [47]. This is in good consistent with the results of alkyl-passivated Si NCs. The C 1s XPS spectrum can be well fitted through two Gaussian peaks at ~ 284.5 and 286.3 eV, corresponding well to C–H and Si–C bonds, respectively [32, 48]. The XPS results further demonstrate that the surface of Si NCs prepared in 1-octadecene by PLA has

been well passivated by organic molecules, in good agreement with FTIR results (in figure 3(a)).

The surface coverage of Si NCs by organic molecules can be estimated to obtain the passivation effect. Taking S4 as an example, the ratio of the integral area of Si 2p peak to that of Si–C bonds centered at 286.2 eV in C 1s XPS spectrum is 4.2. According to M Rosso-Vasic [43], the number of Si atoms for a Si NC with mean diameter 2.37 nm is 278. So, there are around 66 Si–C bonds on Si NCs surface, and the number of surface sites is estimated to be around 117. Hence, the surface coverage of Si NCs with organic molecules is about 58.2%. The surface coverage of Si NCs with organic molecules is about 67.3%, 61.8%, 59.5%, and 58.2% for samples S1–S4, respectively. This is due to the broken of some Si–C bonds under the extreme non-equilibrium conditions when inputting the high laser energy.

The UV–vis absorption spectra of all samples in figure 4(a) appear to have a broad continuous absorption band in the visible region together with a shoulder at around 3.3 eV, similar to the previous published research works on Si NCs [49–51]. The photon energy of 3.3 eV is very close to the direct transition at Γ -point (3.4 eV, $\Gamma_{25} \rightarrow \Gamma_{15}$). The blue-shift of absorption edge of Si NCs compared with that of bulk Si (~ 1.1 eV) is ascribed to an effect of QCE. The optical band gap of colloidal Si NCs can be deduced by Tauc extrapolation for an indirect transition to be about 2.6, 2.4, 2.3 and 2.1 eV

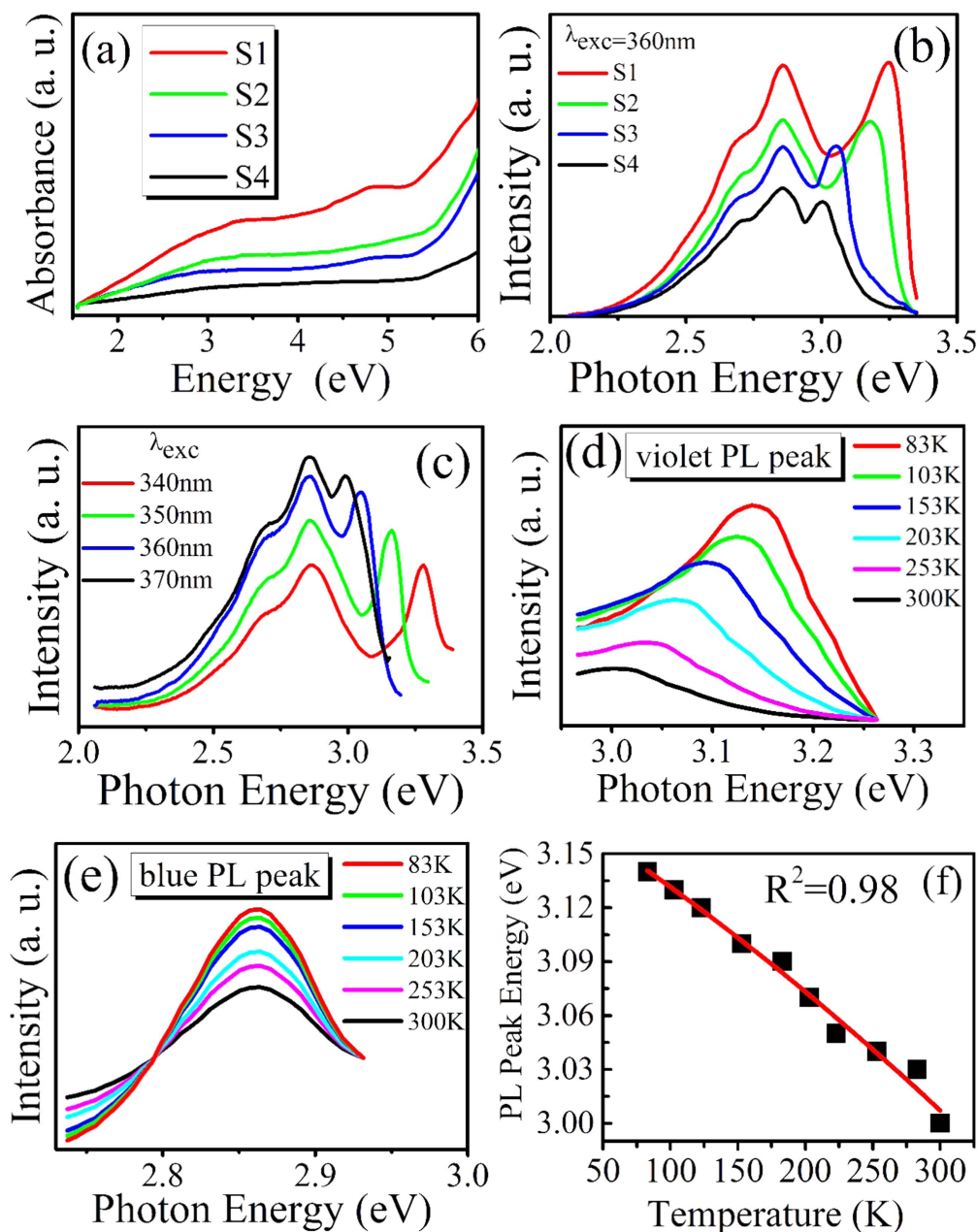


Figure 4. (a) UV–visible absorption spectra of colloidal Si NCs samples, (b) room-temperature PL spectra with excitation wavelength 360 nm of all samples, (c) room-temperature PL spectra of S3 at the indicated λ_{exc} , temperature-dependent PL spectra of S3: (d) violet emission and (e) blue luminescence, and (f) the fitting plot of the violet PL emission peak of S3 against temperature value.

for S1–S4, respectively, further suggesting the existence of QCE. In the visible region, it is evident that a stronger absorption can be observed for colloidal Si NCs prepared at lower laser fluence, compared with those obtained at higher laser fluence. The fabricated colloidal Si NCs with several nanometers diameter is much smaller than the investigated absorption light wavelength, light scattering can be safely neglected. Therefore, the absorbance is supposed to be proportional to the yield of Si NCs. Stronger absorption suggests that there are more Si nanoparticles at lower laser fluence than those under higher laser fluence [24, 51, 52].

Figure 4(b) presents the room temperature PL spectra with excitation wavelength (λ_{exc}) 360 nm for all samples. We can

clearly observe that there are two PL peaks from violet to blue light range for all samples. Moreover, violet and blue emission peaks present different dependence on the laser fluence. There is an obvious redshift for violet luminescence peak from around 3.25 eV in S1 to 3.00 eV in S4, while blue PL emission peak energy at 2.86 eV keeps almost unchanged for these samples. No luminescence can be observed from 1-octadecene alone illuminated by light, indicating that two PL bands should originate from colloidal Si NCs rather than 1-octadecene.

The λ_{exc} - and temperature-dependent PL spectra were carried out to investigate the origin of the luminescence in figure 4(b). Figures 4(c)–(e) illustrate the λ_{exc} and temperature-dependent PL spectra of S3 as a representative,

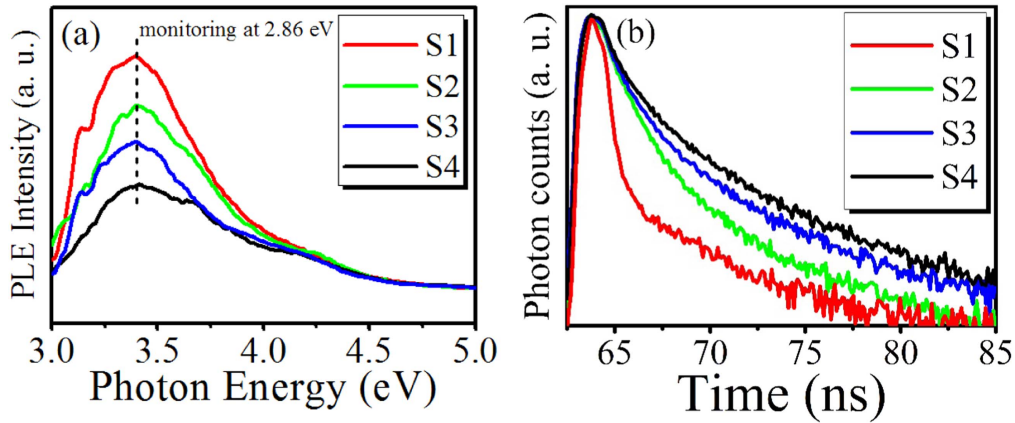


Figure 5. (a) PLE spectra and (b) time-resolved PL spectra detected at 4.86 eV for S3.

respectively. It can be found that the violet emission peak energy presents a remarkable redshift with increasing λ_{exc} and temperature, whereas the blue emission peak energy at 2.86 eV is independent of the λ_{exc} and temperature. Therefore, it is rational to deduce that there are different emission mechanisms contributing to violet and blue emission.

We begin with the investigation of violet light mechanism. (i) Due to QCE, the optical bandgap of Si NCs decreases with the increase of size as determined from UV–vis absorption spectra. More and more small size colloidal Si NCs cannot be excited with the enhancement of λ_{exc} , resulting in redshift of PL emission peak energy [53]. (ii) The temperature-dependent PL peak energy presents a remarkable redshift owing to the decreasing energy gap of colloidal Si NCs with the increase of temperature. These observations suggest that the violet emission originates from the band-to-band direct recombination of electron–holes pairs in quantum confined colloidal Si NCs. Figure 4(f) displays the variation of PL peak energy of S3 as a function of temperature, which could be reproduced by Varshni formula [36, 54]: $E_g(T) = E_0^{\text{bulk}} - \alpha T^2 / (T + \beta)$, where α is the temperature coefficient (dE_g/dT), β is close to the Debye temperature, E_0^{bulk} is the bandgap of bulk Si at 0 K (=1.17 eV). The temperature dependence of PL peak energy is mainly due to the electron–phonon coupling, which leads to the shrink of the semiconductor band gaps with the increase of temperature, resulting in the redshift of PL emission [55]. For blue emission, considering the observation of λ_{exc} and temperature independent PL peak position, we will assign later that the luminescence is related to the localized excitons’ radiative recombination via the oxygen-related surface states on the surface of the colloidal Si NCs.

In addition, both violet and blue PL bands intensity of samples decreases with the increase of temperature from 83 to 300 K. The similar temperature-dependent behaviors of PL bands intensity have been reported in colloidal Si NCs passivated with Si–C bonding [56]. This indicates that the radiative recombination processes dominate at low temperature, while the non-radiative recombination centers become thermally activated with the enhancement of temperature, resulting in the decreases of PL intensity.

Now we focus on the effect of laser fluence on blue PL bands. Figure 5(a) displays the PLE spectra of all the samples with the detection energy of 2.86 eV. The PLE peak position at 3.30 eV is independent of laser fluence, which is slightly smaller than the experimental Γ -point interband transition energy of 3.4 eV of bulk Si [57]. According to the theoretical modeling of Si NCs, the 0.1 eV redshift of the interband transition energy compared to bulk Si is attributed to QCE [58]. The quantum size confinement effect will not only influence the optical bandgap value, but also the direct transition energy at Γ -point [59]. However, the direct transition energy at Γ -point is size-dependent, and should also shift with the variation of size in Si NCs. According to Rama Krishna, *et al* the direct transition energy at Γ -point will first increase slightly with the reduction of the Si crystal size and then decrease [59]. They have reported that the direct transition energy at Γ -point increases from 3.39 to 3.40 eV with the increase of Si NCs size from 50 to 25 nm. When further decreasing Si NCs to 6.5 nm, and the corresponding direct transition energy at Γ -point drops to 3.14 eV. On the basis of the above discussions, the possible origin of blue emission from the direct transition at Γ -point can be safely ruled out in our case. Compared with the PL peak energy 2.86 eV, the PLE peak energy (3.30 eV) has an obvious Stokes shift of 0.44 eV, demonstrating that the carriers have been mostly generated at the energy level of 3.3 eV [60].

To understand the recombination mechanism of carriers in Si NCs, time-resolved PL spectra were measured for all samples. Figure 5(b) displays the decay curves of all samples recorded at an emission peak of 2.86 eV. All the decay curves can be calculated through double-exponential iterative fitting program provided by Edinburgh Instruments. It can be found that the experimental data can be well fitted using double-exponential function [32]: $I(t) = A_1 e^{-t/\tau_1} + A_2 e^{-t/\tau_2}$, where $I(t)$ is the PL intensity as a function of time t ; A_1 , A_2 , τ_1 and τ_2 are the fitting constants. The colloidal Si NCs exhibit characteristic lifetimes with a fast decay component from 0.93 to 1.25 ns and a slow one from 4.78 to 5.36 ns, with the increase of laser fluence from 1.0 to 2.5 mJ cm^{-2} . The average lifetime $\bar{\tau}$ can be calculated by using the equation: $\bar{\tau} = (A_1 \tau_1^2 + A_2 \tau_2^2) / (A_1 \tau_1 + A_2 \tau_2)$, the obtained $\bar{\tau}$ increases from 3.6 ns in S1 to 5.2 ns in S4 with the increase of laser

fluence. Due to the stronger QCE in smaller Si NCs than that in large ones, the radiative recombination rate enhances and the decay lifetime of the order of nanoseconds decreases in smaller Si NCs size.

It is reported that the following PL mechanisms are often used to explain the fast blue PL in Si NCs: (i) The first one is attributed to the direct bandgap recombination of electrons-holes pairs at Γ point. (ii) The second one is the excitons recombination in Si NCs with certain modified surface [61]. (iii) The third one is related to oxygen-related surface states, PL peak value will keep fixed when excited by different wavelength [33]. The direct recombination of electrons-holes at Γ point can be safely excluded due to the size-dependent transition in Si NCs, and the PL peak energy has to be a blue shift with the size reduction of Si NCs [62]. In this case, the Si=O bonds may introduce localized states in the Si NCs due to the oxidation of the Si nanocrystal's surface [63]. According to the First-principle, the nanosecond decay time can be attributed to the localized state exciton transitions on the surface of the Si NCs [33]. The oxygen-related surface states acting as the radiative recombination centers to give rise to blue emission in Si NCs has been reported in previous works [32, 64, 65]. Based on these analyses, we propose that the blue emission originates from the radiative recombination of the localized excitons generated at 3.3 eV energy level via oxygen-related surface states on the surface of the colloidal Si NCs.

Finally, we discuss the decrease of the PL intensity with the increase of laser fluence. On one hand, due to the broken of the Si–O and Si–C bonds at higher laser fluence (see figure 3(b)), the dangling bonds acting as non-radiative recombination centers cannot be well passivated; On the other hand, the aggregated Si NCs at high laser fluence results in the decrease of Si NCs density, as deduced from UV–vis absorption spectra (figure 4(a)), thus there are fewer excited electron–hole pairs can be transferred to the surface of Si NCs to recombine.

In summary, XRD, Raman scattering, HRTEM, FTIR, and XPS measurements have been employed to reveal the evolution of the structure, chemical compositions, and bonding environment of the colloidal Si NCs with the laser fluence. Through analyzing the UV–vis absorption, λ_{exc} /temperature-dependent PL spectra, the size-dependent spectral shift of violet emission is attributed to the QCE. In combination with the time-resolved PL and PLE spectra, we attribute the origin of the blue luminescence to the localized excitons' radiative recombination via oxygen-related surface states on the surface of colloidal Si NCs. Based on the understanding the violet and blue emitting mechanism from colloidal Si NCs, the convenient and environment-friendly synthesis routes can be further popularized to replace time-consuming ones to fabricate the stable colloidal Si NCs, which can facilitate their applications in optoelectronic devices.

Acknowledgments

This work was financially supported by the National Natural Science Foundation of China (Grant No. 11504229 and 61234005).

ORCID iDs

H L Hao  <https://orcid.org/0000-0003-3341-5731>

References

- [1] Walters R J, Bourianoff G I and Atwater H A 2005 *Nat. Mater.* **4** 143
- [2] Maier-Flaig F, Rinck J, Stephan M, Bocksrocker T, Bruns M, Kübel C, Powell A K, Ozin G A and Lemmer U 2013 *Nano Lett.* **13** 475
- [3] Gu W et al 2017 *IEEE Photonics J.* **9** 4500610
- [4] Yu T, Wang F, Xu Y, Ma L L, Pi X D and Yang D R 2016 *Adv. Mater.* **28** 4912
- [5] Beard M C, Knutsen K P, Yu P R, Luther J M, Song Q, Metzger W K, Ellingson R J and Nozik A J 2007 *Nano Lett.* **7** 2506
- [6] Liu C Y, Holman Z C and Kortshagen U R 2010 *Adv. Funct. Mater.* **20** 2157
- [7] Ding Y, Gresback R, Liu Q M, Zhou S, Pi X D and Nozaki T 2014 *Nano Energy* **9** 25
- [8] Zhao S Y, Pi X D, Mercier C, Yuan Z C, Sun B Q and Yang D R 2016 *Nano Energy* **26** 305
- [9] Fujioka K et al 2008 *Nanotechnology* **19** 415102
- [10] Gross E, Kovalev D, Künzner N, Diener J, Koch F, Timoshenko V Y and Fujii M 2003 *Phys. Rev. B* **68** 115405
- [11] Zhong Y L, Sun X T, Wang S Y, Peng F, Bao F, Su Y Y, Li Y Y, Lee S T and He Y 2015 *ACS Nano* **9** 5958
- [12] Ghosh B and Shirahata N 2014 *Sci. Technol. Adv. Mater.* **15** 014207
- [13] Besner S, Kabashin A V, Winnik F M and Meunier M 2008 *Appl. Phys. A* **93** 955
- [14] Zeng H B, Du X W, Singh S C, Kulinich S A, Yang S K, He J P and Cai W P 2012 *Adv. Funct. Mater.* **22** 1333
- [15] Shirahata N, Hirakawa D and Sakka Y 2010 *Green Chem.* **12** 2139
- [16] Yuan Z, Nakamura T, Adachi S and Matsuishia K 2017 *Nanoscale* **9** 1193
- [17] Shirahata N, Hirakawa D, Masuda Y and Sakka Y 2013 *Langmuir* **29** 7401
- [18] Sumi T, Motono S, Ishida Y, Shirahata N and Yonezawa T 2015 *Langmuir* **31** 4323
- [19] Porta M, Nguyen M T, Tokunaga T, Ishida Y, Liu W R and Yonezawa T 2016 *Langmuir* **32** 12159
- [20] Yang S K, Cai W P, Zhang H W, Xu X X and Zeng H B 2009 *J. Phys. Chem. C* **113** 19091
- [21] Chewchinda P, Tsuge T, Funakubo H, Odawara O and Wada H 2013 *Japan. J. Appl. Phys.* **52** 025001
- [22] Kuzmin P G, Shafeev G A, Bukin V V, Garnov S V, Farcau C, Carles R, Warot-Fontrose B, Guieu V and Viau G 2010 *J. Phys. Chem. C* **114** 15266
- [23] Intartaglia R, Bagga K, Brandi F, Das G, Genovese A, Di Fabrizio E and Diaspro A 2011 *J. Phys. Chem. C* **115** 5102
- [24] Hamad S, Krishna P G, Vendamani V S, Nageswara R S V S, Pathak A P, Tewari S P and Venugopal R S 2014 *J. Phys. Chem. C* **118** 7139
- [25] Chewchinda P, Odawara O and Wada H 2014 *Appl. Phys. A* **117** 131
- [26] Angt A, Sinelnikov R, Meldrum A, Veinot J G C, Balberg I, Azulay D, Millo O and Rieger B 2016 *Nanoscale* **8** 7849
- [27] Wang R, Pi X D and Yang D R 2012 *J. Phys. Chem. C* **116** 19434
- [28] Vincenzo A and Moreno M 2009 *Phys. Chem. Chem. Phys.* **11** 3805

- [29] Hwang D J, Grigoropoulos C P and Choi T Y 2006 *J. Appl. Phys.* **99** 083101
- [30] Švrček V, Sasaki T, Katoh R, Shimizu Y and Koshizaki N 2009 *Appl. Phys. B* **94** 133
- [31] Nakamura T, Yuan Z and Adachi S 2014 *Nanotechnology* **25** 275602
- [32] Tan D Z, Ma Z J, Xu B B, Dai Y, Ma G H, He M, Jin Z M and Qiu J R 2011 *Phys. Chem. Chem. Phys.* **13** 20255
- [33] Hao H L and Shen W Z 2008 *Nanotechnology* **19** 455704
- [34] Henderson E J, Kelly J A and Veinot J G C 2009 *Chem. Mater.* **21** 5426
- [35] Hessel C M, Reid D, Panthani M G, Rasch M R, Goodfellow B W, Wei J W, Fujii H, Akhavan V and Korgel B A 2012 *Chem. Mater.* **24** 393
- [36] Ghosh B, Takeguchi M, Nakamura J, Nemoto Y, Hamaoka T, Chandra S and Shirahata N 2016 *Sci. Rep.* **6** 36951
- [37] Duan Y, Kong J F and Shen W Z 2012 *J. Raman Spectrosc.* **43** 756
- [38] Hessel C M, Wei J W, Reid D, Fujii H, Downer M C and Korgel B A 2012 *J. Phys. Chem. Lett.* **3** 1089
- [39] Zi J, Zhang K M and Xie X D 1997 *Phys. Rev. B* **55** 9263
- [40] Paillard V, Puech P, Laguna M A, Carles R, Kohn B and Huisken F 1999 *J. Appl. Phys.* **86** 1921
- [41] Inada M, Nakagawa H, Umezu I and Sugimura A 2002 *Appl. Surf. Sci.* **197-198** 666
- [42] Shirahata N, Linford M R, Furumi S, Pei L, Sakka Y, Gates R J and Asplund M C 2009 *Chem. Commun.* **31** 4684
- [43] Rosso-Vasic M, Spruijt E, van Lagen B, De Cola L and Zuilhof H 2008 *Small* **4** 1835
- [44] Canaria C A, Lees I N, Wun A W, Miskelly G M and Sailor M J 2002 *Inorg. Chem. Commun.* **5** 560
- [45] Kúsová K et al 2010 *Acs Nano* **4** 4495
- [46] Mangolini L and Kortshagen U 2007 *Adv. Mater.* **19** 2513
- [47] Llansola P M J, Nieto F R, Soria D B, Amalvy J I, Peruzzo P J, Mártire D O, Kotler M, Holub O and Gonzalez M C 2009 *J. Phys. Chem. C* **113** 13694
- [48] Wang Q, Ni H J, Pietzsch A, Hennies F, Bao Y P and Chao Y M 2011 *J. Nanopart. Res.* **13** 405
- [49] Intartaglia R, Bagga K, Scotto M, Diaspro A and Brandi F 2012 *Opt. Mater. Express* **2** 510
- [50] Vaccaro L, Sciortino L, Messina F, Buscarino G, Agnello S and Cannas M 2014 *Appl. Surf. Sci.* **302** 62
- [51] Li X, Zhang G M, Jiang L, Shi X S, Zhang K H, Rong W L, Duan J and Lu Y F 2015 *Opt. Express* **23** 4226
- [52] Yuan Z, Nakamura T, Adachi S and Matsuishi K 2017 *J. Phys. Chem. C* **121** 8623
- [53] Lu W B, Wu L P, Yu W, Wang X Z, Li X W and Fu G S 2012 *Micro Nano Lett.* **7** 1125
- [54] Niu Y W, Zhang F, Bai Z L, Dong Y P, Yang J, Liu R B, Zou B S, Li J B and Zhong H Z 2015 *Adv. Opt. Mater.* **3** 112
- [55] Varshni Y P 1967 *Physica* **34** 149
- [56] Chao Y, Houlton A, Horrocks B R, Hunt M R C, Poolton N R J, Yang J and Šiller L 2006 *Appl. Phys. Lett.* **88** 263119
- [57] Adachi S 1988 *Phys. Rev. B* **38** 12966
- [58] Prokofiev A A, Moskalenko A S, Yassievich I N, de Boer W D A M, Timmerman D, Zhang H, Buma W J and Gregorkiewicz T 2009 *JETP Lett.* **90** 758
- [59] Rama Krishna M V and Friesner R A 1992 *J. Chem. Phys.* **96** 873
- [60] Yamaguchi K, Mizushima K and Sassa K 2000 *Appl. Phys. Lett.* **77** 3773
- [61] Xu Y M and Han Y H 2014 *Appl. Phys. A* **117** 1557
- [62] De Boer W D A M, Timmerman D, Dohnalová K, Yassievich I N, Zhang H, Buma W J and Gregorkiewicz T 2010 *Nat. Nanotechnol.* **5** 878
- [63] Wang M H, Yang D R, Li D S, Yuan Z Z and Que D L 2007 *J. Appl. Phys.* **101** 103504
- [64] Saitow K and Yamamura T 2009 *J. Phys. Chem. C* **113** 8465
- [65] Pi X D, Liptak R W, Deneen Nowak J, Wells N P, Carter C B, Campbell S A and Kortshagen U 2008 *Nanotechnology* **19** 245603